Absorption-Induced Separations in Oscillatory Liquid Chromatography

Yolanda M. M. Van Lishout and David T. Leighton, Jr.
Dept. of Chemical Engineering, University of Notre Dame, Notre Dame, IN 46556

It has been shown that small-amplitude oscillations can augment the diffusional flux across a cylindrical tube by several orders of magnitude through Taylor – Aris dispersion phenomena (Aris, 1960). This enhancement in mass transport is selective for species with different molecular diffusion coefficients. This article shows that by coupling fluid oscillations with a reversible absorption in a stationary phase, the transport of species, which have similar molecular diffusivities but different affinities for the stationary phase, can be enhanced selectively. We developed analytical and asymptotic solutions to the enhancement of mass transfer as a result of the interaction between reversible absorption and fluid oscillations in a cylindrical tube. These results were qualitatively confirmed by experiments with a model system. For purely oscillatory flow, the maximum selectivity (the ratio of the fluxes of the species to be separated) achievable is 4.4 for solute species with widely different affinities for the stationary phase. The superposition of a small-amplitude steady backflow, however, can greatly increase the selectivity, but at the expense of throughput. Analysis shows that this technique may offer improvements relative to conventional liquid membrane separations, if the solute affinities for the stationary phase do not greatly differ or if a thick membrane is required for stability.

Introduction

Recently it has been demonstrated (Leighton and McCready, 1988; Chandhok et al., 1990) that the rate of mass transfer across a supported liquid membrane can be greatly enhanced by inducing membrane fluid oscillations in the pores of the support. This enhancement mechanism relies on the coupling between radial diffusion across each pore with oscillatory axial convection (Aris, 1960). The enhancement in diffusion across a membrane can be very substantial—a tidal oscillation of no more than the pore radius doubles the transport rate, and larger oscillations can increase the rate by several orders of magnitude. This enhancement in transport has been experimentally verified in our laboratory (Chandhok et al., 1990; Chandhok and Leighton, 1991). Over 200-fold increases in mass transfer have been observed, and much greater enhancements are possible with suitably designed membrane supports. The transport enhancement is governed by the dimensionless parameter $\omega a^2/D$, where ω is the oscillation frequency, a is the pore radius, and D is the molecular diffusivity. If this parameter is large (such as is typical for low-diffusivity molecules), the enhancement will occur. If it is small, then the enhancement in mass transfer will be absent. Thus, by appropriate choice of the oscillation frequency, it is possible to enhance the mass transport rate of low-diffusivity species selectively. Note that enhancement is nonselective for species with similar diffusivities.

The absorption-induced separation technique we describe here builds on our previous work in this area. As mentioned, the interaction between fluid oscillations along the length of a tube and diffusion across the tube can lead to a substantial increase in the mass transfer. If the species is capable of being absorbed into a stationary phase, it is possible to modify the frequency dependence of this mass-transfer enhancement significantly. It is possible to regulate the frequency such that, for species that have different affinities for the stationary phase, the species that absorbs more strongly experiences a greater rate of enhancement. The oscillation frequency is chosen so that the enhancement due to absorption is large, but the enhancement in the mobile phase (which, in this case, is not selective) is minimized. If diffusion into the stationary

Correspondence concerning this article should be addressed to D. T. Leighton, Jr.

phase is much slower than diffusion in the mobile phase, this condition is easily achieved.

In the next section, we develop a model for the selective enhancement in transport by coupling a reversible absorption in a stationary phase to fluid oscillations. This mass transport enhancement is closely related to the dispersion or peak spreading encountered in conventional liquid chromatography. In fact, the technique described here may be best understood as an oscillatory liquid chromatography system in which the dispersion for one species has been enhanced so much that it leads to a steady mass flux between reservoirs at the ends of the chromatographic column. The column itself, when operated in this manner, can thus be regarded as a perm-selective membrane.

In the third section, we describe the experiments that verify the separation approach. As a model system, we separate 1-butanol and *t*-butanol from an aqueous solution with *n*-octanol incorporated in the stationary phase. 1-Butanol and *t*-butanol were chosen since they have the same diffusivity but different partition coefficients for *n*-octanol. In the fourth section, we give the results of the analysis of the experimental data. We discuss the scaling laws that govern the separation technique and that allow for a comparison of this technique to separations with an ordinary membrane in the fifth section. The final section provides a summary of our results and conclusions.

Theory

The interaction of the fluid oscillations and the reversible absorption in the stationary phase giving rise to a selective increase of mass transfer is depicted in Figure 1. A solution for the analogous problem, the enhancement of thermal diffusivity due to the interaction of wall conduction and fluid oscillation, was obtained by Kurzweg (1985). He developed a formal solution for the enhanced axial thermal diffusivity κ_e as a function of the Womersley number α, the fluid Prandtl number Pr, and the ratio of the fluid and wall thermal conductivities κ for the case of viscous fluid oscillations within parallel-plate channels. Here the Womersley number $\alpha \equiv (\omega a^2/\nu)^{1/2}$, where ω is the angular frequency of oscillation, $2a$ is the gap width, and ν is the kinematic viscosity, is a measure of the effect of fluid inertia on the velocity profile.

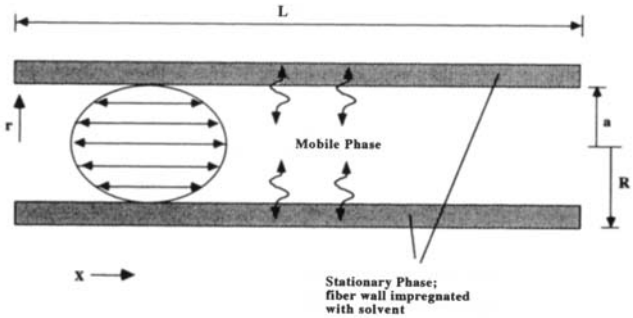

Figure 1. Transport enhancement in a hollow fiber due to coupling fluid oscillations and reversible selective absorption in the stationary phase.

The driving force for the radial diffusion is the radial concentration gradient across the two phases that changes direction as the fluid oscillates.

Kurzweg also presented the asymptotic expressions for κ_e at very high frequency where α and $\alpha^2 Pr$ are large, and at low frequency where α, $\alpha^2 Pr$ and $\zeta\alpha\sqrt{\kappa Pr}$ are small (ζ is the ratio of the channel wall thickness to the channel half-width). These asymptotic solutions, however, are not applicable to mass-transfer enhancement in a liquid membrane. In the case of a liquid membrane the Schmidt number σ (which plays the same role as does the Prandtl number in the corresponding energy transfer problem) is very large and it is more appropriate to examine the mass transport as a function of $\beta = \alpha\sigma^{1/2}$ (Leighton and McCready, 1988). In this case α is small even for large values of β, and fluid inertia is unimportant.

In our work we solve the analogous problem, the selective enhancement of transport due to the interaction of reversible absorption in the stationary phase and fluid oscillations, for cylindrical tubes, and develop a formal solution for the enhanced axial molecular diffusivity as well as the asymptotic expressions for large and small β. The stationary phase is modeled as a bundle of hollow fibers of length L, inner radius a, and outer radius R (Figure 1). Such hollow-fiber systems (in which the volume outside the fibers plays no role) have been proposed for conventional liquid chromatography (Ding et al., 1989). Here we are using the hollow fibers with oscillatory rather than steady flow. The porous fiber walls can be impregnated with a membrane fluid that selectively absorbs a solute species. In the experiments described in the next section, for example, the porous walls are impregnated with *n*-octanol, and preferentially absorb 1-butanol relative to *t*-butanol, providing the basis for their separation.

To solve the problem analytically, we make several simplifying assumptions. We assume the solution is dilute such that the diffusivity and the density are constant. The transport equation for the solute in the mobile phase, neglecting the small contribution due to axial molecular diffusion, is

$$\frac{\partial C}{\partial t} + U\cos(\omega t)\frac{\partial C}{\partial x} = D\frac{1}{r}\frac{\partial}{\partial r}\left(r\frac{\partial C}{\partial r}\right), \tag{1}$$

where D is the molecular diffusivity and ω is the angular frequency of the fluid oscillations. The contribution due to axial molecular diffusion can be easily included in the analysis. For large-amplitude oscillations, however, axial diffusion is negligible compared to the dispersion arising from the fluid motion. The velocity profile for laminar flow and small Womersley number, neglecting end effects present at points where the fibers enter the source and receiving reservoirs, is given as

$$U = 2\overline{U}\left[1 - \left(\frac{r}{a}\right)^2\right], \tag{2}$$

where $\overline{U}$ is the spatially averaged magnitude of the oscillatory velocity. The transport equation for the stationary phase, again neglecting axial diffusion, is given as

$$\frac{\partial C_s}{\partial t} = D_s\frac{1}{r}\frac{\partial}{\partial r}\left(r\frac{\partial C_s}{\partial r}\right), \tag{3}$$

where here C_s is the superficial concentration of the solute in the stationary phase and D_s is some effective molecular

diffusivity in the radial direction. The effective molecular diffusivity can be obtained from conventional membrane transport resistance measurements at steady state in which the membrane is made up of the same materials as the stationary phase in an oscillatory system.

The interface between the stationary and mobile phases is assumed to be locally at equilibrium; thus, we have

$$\phi C_s|_{r=a^+} = C|_{r=a^-}, \tag{4}$$

where ϕ is the partition coefficient. The partition coefficient is defined as the ratio of the concentration of the solute in the mobile phase to the superficial concentration of the solute in the stationary phase. Mass flux balances at the centerline, interface, and outer fiber wall lead to the final boundary conditions

$$D\left.\frac{\partial C}{\partial r}\right|_{r=a^-} = D_s\left.\frac{\partial C_s}{\partial r}\right|_{r=a^+}, \quad \left.\frac{\partial C}{\partial r}\right|_{r=0} = 0, \quad \left.\frac{\partial C_s}{\partial r}\right|_{r=R} = 0. \tag{5}$$

In the past, two methods have been used to obtain an analytical expression for the effective diffusivity. Kurzweg (1985) and Watson (1983) developed a solution by imposing a time-averaged constant axial gradient with a time-dependent cross-stream variation and solving for the time-averaged convective flux. In contrast, Aris (1960) studied the time-dependent dispersion of solute, initially confined to a cross-stream plane of uniform concentration, via the method of moments. For the case of purely oscillatory flow, the effective diffusivity calculated by these two methods is identical. In our work, we have chosen to use the methods of moments. We refer the reader to the Appendix for details of the derivation. We define an enhanced axial diffusivity K by the throughput relationship $Q = \pi a^2 K \Delta C/L$, where Q is the time-averaged throughput of a solute species between two reservoirs at concentrations differing by ΔC, connected by a fiber of length L and radius a. The solution for the enhanced axial diffusivity is given by

$$K = 4\frac{\Delta x^2 \omega}{\beta^2} \times \left(1 - Re\left\{B\left[\frac{4}{\sqrt{2}\beta^3} J_1(i^{3/2}\beta)(1-i) - \frac{2i}{\beta^2} J_0(i^{3/2}\beta)\right]\right\}\right), \tag{6}$$

where

$$B = \frac{\phi\sqrt{\lambda}\,\beta\sqrt{2}\,(1+i)G + 4H}{J_0(i^{3/2}\beta)H - i\sqrt{\lambda}\,\phi J_1(i^{3/2}\beta)G}$$

$$H = J_1(i^{3/2}\sqrt{\lambda}\,\epsilon\beta)K_1(i^{1/2}\sqrt{\lambda}\,\beta) - J_1(i^{3/2}\sqrt{\lambda}\,\beta)K_1(i^{1/2}\sqrt{\lambda}\,\epsilon\beta)$$

$$G = J_1(i^{3/2}\sqrt{\lambda}\,\epsilon\beta)K_0(i^{1/2}\sqrt{\lambda}\,\beta) + iJ_0(i^{3/2}\sqrt{\lambda}\,\beta)K_1(i^{1/2}\sqrt{\lambda}\,\epsilon\beta),$$

where ϵ is the ratio of the outer radius to the inner radius ($\epsilon = R/a$), λ is the ratio of the mobile phase-to-stationary phase molecular diffusivities ($\lambda = D/D_s$), and $\Delta x = \bar{U}/\omega$ is the tidal displacement of the fluid oscillation. The functions $J_n(i^{3/2}y)$ and $K_n(i^{1/2}y)$ are Bessel functions related to the Kelvin functions ber, bei, ker, and kei by $J_n(i^{3/2}y) = \mathrm{ber}_n(y) + i\,\mathrm{bei}_n(y)$ and $K_n(i^{1/2}y) = e^{n\pi i/2}\,[\mathrm{ker}_n(y) + i\,\mathrm{kei}_n(y)]$.

In order to study the enhancement due to the coupling of absorption in the stationary phase and fluid oscillations, we have obtained analytical expressions for the asymptotic solutions of the enhanced axial diffusion coefficient. The expression for small β is

$$K = \frac{\Delta x^2 \omega}{96} \frac{\left[11(1-\epsilon^2)^2 + 24\phi\lambda\epsilon^2(1+\epsilon^2\ln\epsilon) + \phi^2 - 6\phi(1+\lambda) + 6\phi\epsilon^2(1-3\lambda\epsilon^2)\right]}{(\phi - 1 + \epsilon^2)^2}\beta^2 + 0(\beta^4) \tag{7}$$

and the asymptotic limit for large β is

$$K = 4\frac{\Delta x^2 \omega}{\beta^2}\left[1 - \frac{2\sqrt{2}}{\beta}\frac{\phi\sqrt{\lambda}}{(1+\phi\sqrt{\lambda})} + O\left(\frac{1}{\beta^2}\right)\right] \qquad \beta(\epsilon-1)\sqrt{\lambda} \gg 1. \tag{8}$$

Note that for $\phi\sqrt{\lambda} \gg 1$ (no wall absorption) the high-frequency limit reduces to Watson's (1983) result in the limit of small α and large β. Watson studied the enhancement of transport due to fluid oscillations—without wall absorption—for conduits of arbitrary shape. Watson's result for a cylinder, in the limit of small α, as a function of β is given as follows

$$K = 4\frac{\Delta x^2 \omega}{\beta^2}\left(1 - 2\sqrt{2}\,Re\left\{\frac{1+i}{\beta}\frac{J_0(i^{3/2}\beta)}{J_1(i^{3/2}\beta)}\right\}\right). \tag{9}$$

Figure 2 shows the full solution for the enhanced axial diffusivity as well as the asymptotic limits for small and large β and Watson's solution for the enhancement due to Taylor–Aris dispersion in the mobile phase only, which, as mentioned before, is nonselective for species with the same molecular diffusivity. It may be seen that there are two distinct frequency ranges in which the transport is enhanced due to different mechanisms. In the low-frequency region [$\beta < O(1)$] the interaction of the absorption in the stationary phase and the fluid oscillations clearly dominates the transport enhancement. The asymptotic solution for the low-frequency limit, which contains the parameters ϵ, ϕ, and λ that govern the effect of the wall on the enhancement, describes this regime fairly well. The difference between the full solution and Watson's solution is the selective increase in dispersion due to absorption. The selectivity is a result of the differences in affinity that species have for the stationary phase. At very high frequencies [$\beta \geq O(10)$] the stationary phase has little or no effect, as can be seen from the convergence of the asymptotic solution at high frequencies with the nonselective enhancement in the mobile phase studied by Aris (1960) and Watson (1983). In contrast to the low-frequency limit, at high frequencies diffusion is slow with respect to the convective oscillations, and a radial concentration gradient develops in

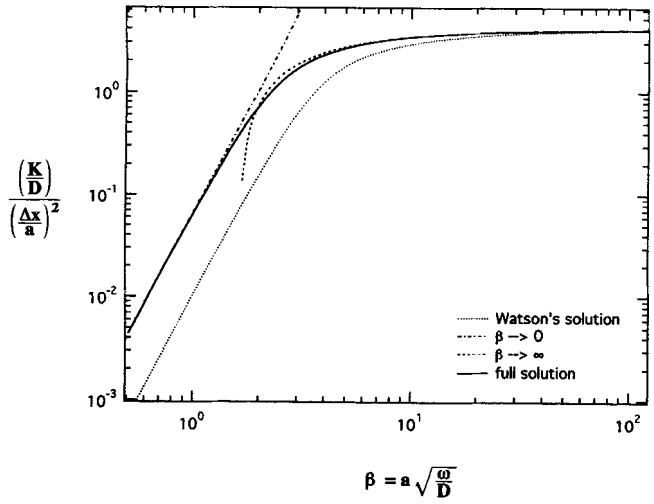

Figure 2. Nondimensionalized, enhanced axial diffusivity K as a function of the nondimensional oscillation frequency β for parameter values of our experimental model system.

$\lambda = 61$, $\epsilon = 1.25$, $\phi = 0.54$.

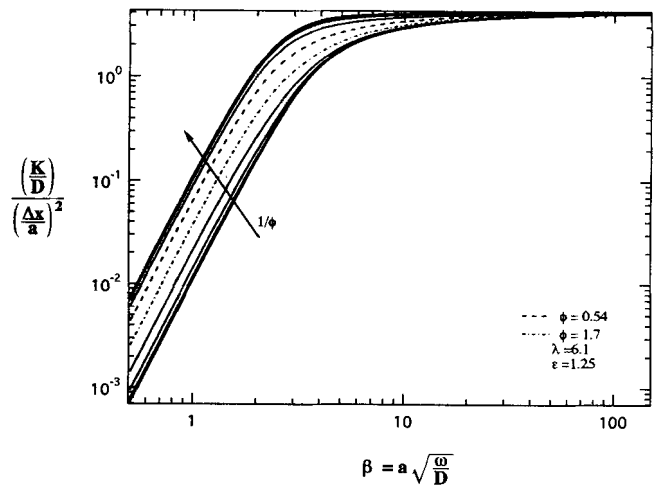

Figure 3. Nondimensionalized enhanced axial diffusivity K as a function of the nondimensional oscillation frequency β, where each curve was parameterized by the partition coefficient ϕ such that the ratio of ϕ of two neighboring curves is constant.

The partition coefficients of the dashed curves are those of the two species of our experimental model system.

the mobile phase. It is the interaction of this radial concentration gradient with convection that gives rise to the nonselective dispersion of the solute.

As mentioned earlier, the parameters ϵ, ϕ, and λ govern the enhancement due to absorption in the stationary phase, and therefore also govern the selectivity of the separation. The dependence of the enhancement on these parameters is very complex. At low frequencies (Eq. 7), for given values of λ and ϵ, increasing the absorptivity, $1/\phi$, can either increase or decrease the relative enhancement of transport. At these frequencies, however, the enhancement in mass transport is rather small and therefore it is of little practical importance. In general, we desire to operate at sufficiently high oscillation frequencies that the enhancement due to reversible absorption is large, but not so high a frequency that the nonselective enhancement due to Taylor–Aris dispersion in the mobile phase alone is also large. The operating frequency at which this is achieved is approximately given by $\beta = 3$. In contrast to the low-frequency region, at these moderately high frequencies (Eq. 8) the thickness of the stationary phase has little effect on the enhancement because the penetration depth $[(D_s/\omega)^{1/2}]$ of the solute is usually less than the stationary phase thickness. The penetration depth is the distance that the solute can diffuse into the stationary phase during an oscillation period. For this condition $[\beta(\epsilon - 1)\sqrt{\lambda} \gg 1]$, the enhancement does not depend on λ and ϕ independently, but rather only on the combination $\phi\sqrt{\lambda}$.

Figure 3 shows the behavior of the enhancement for the parameter values ϵ and λ of our experimental system, where each curve is parameterized by ϕ. While the absolute values of ϕ are different for each curve, the ratio of ϕ for two neighboring curves is held constant. The two dashed curves are those corresponding to the partition coefficients of 1-butanol (0.54) and t-butanol (1.7). Examining the family of curves, it can be seen that at high frequencies the enhancement increases monotonically as a function of $1/\phi$ and exhibits both a minimum and a maximum. Hence, in order to achieve the optimum enhancement and maximum selectivity, it is necessary to operate where one species is absorbed strongly and the other weakly. If both the species absorb either very strongly or weakly, no separation can be achieved. Our experiments were performed near the region giving an optimum enhancement and selectivity.

The maximum degree of selectivity for species whose partition coefficients differ by a factor of 3.1 (the values for our experimental system) is only about 1.6. This is less than the selectivity that would result from a separation with a conventional liquid membrane for which n-octanol is used as the membrane fluid; however, because of the enhancement due to fluid oscillations, the overall transport rate can be much greater. The maximum possible selectivity at high oscillation frequencies for large ratios of ϕ is approximately 4.4.

For many applications the maximum selectivity provided by the oscillatory chromatography technique described here is not sufficient. This selectivity can be improved dramatically by employing a small-amplitude back flow. It has been shown (Hertz, 1923; Jaeger et al., 1992) that a small-amplitude back flow permits a better separation for diffusion in gases. However, the increase in selectivity occurs at the expense of the transport rate across the fiber. Note that it is not possible to incorporate such a back flow in an ordinary liquid membrane since it would result in membrane rupture; thus, the selectivity of such membranes is strictly limited by the relative affinity of the two solute species for the membrane fluid.

The steady time-averaged (over one period of oscillation) flux between two reservoirs connected by a bundle of hollow fibers impregnated with a solvent that selectively absorbs a solute species, as a result of the coupling of fluid oscillations and a small-amplitude steady back flow, is given as

$$N = -\overline{U}_{BF}C - K\frac{\partial C}{\partial x}, \tag{10}$$

where $\overline{U}_{BF}$ is the spatially averaged velocity of the steady back flow and K is the enhanced axial diffusivity due to the coupling of the fluid oscillation and reversible absorption. It is simple to show, using the method of moments (Chandhok, 1992), that the effect of coupling a steady flow and an oscillatory flow on the dispersion of a slug of solute is simply the sum of the dispersion under steady and oscillatory flow. Unfortunately, however, the relationship between dispersion and enhanced axial diffusivity in the case of steady flow and a time-averaged (over one oscillation period) steady concentration gradient is much more complex than the purely oscillatory case. The contribution of the steady back flow to the dispersion due to fluid oscillations will be a function of the ratio $(\overline{U}_{BF}/\overline{U})^2$; therefore, for a sufficiently small steady flow relative to the oscillatory convection, we can neglect the effect of the steady flow on the magnitude of the enhanced diffusion coefficient. In our experiments the magnitude of $(\overline{U}_{BF}/\overline{U})^2$ was on the order of 0.005 or smaller, and no dependence of the enhancement on the magnitude of the back flow was observed.

Diffusion against a low-amplitude back flow gives rise to an exponentially decreasing concentration profile rather than the linear profile that exists in the absence of flow. The concentration gradient can be found by taking the derivative with respect to x (the axial coordinate) and solving the resulting equation

$$\frac{\partial N}{\partial x} = 0 \qquad \therefore K\frac{\partial^2 C}{\partial x^2} + \overline{U}_{BF}\frac{\partial C}{\partial x} = 0 \tag{11}$$

with the boundary conditions

$$x = 0 \quad C = C_o \quad \text{and} \quad x = L \quad C = C_L, \tag{12}$$

where C_o and C_L are the concentrations at the ends of the fibers connecting the reservoirs, and L is the length of the fibers. The resulting concentration profile is given by

$$C = \frac{C_L\left[1-\exp\left(-\frac{x\overline{U}_{BF}}{K}\right)\right] + C_o\left[\exp\left(-\frac{x\overline{U}_{BF}}{K}\right) - \exp\left(\frac{L\overline{U}_{BF}}{K}\right)\right]}{1-\exp\left(-\frac{L\overline{U}_{BF}}{K}\right)}. \tag{13}$$

The rate by which the concentration gradient decreases depends on the magnitude of the modified Peclet number $\chi = L\overline{U}_{BF}/K$. Substituting Eq. 13 into Eq. 11 gives us the final expression for the flux along the fibers:

$$N = \overline{U}_{BF}\frac{C_o - C_L\exp\left(\frac{L\overline{U}_{BF}}{K}\right)}{\exp\left(\frac{L\overline{U}_{BF}}{K}\right)-1}. \tag{14}$$

The selectivity is defined as the ratio of the time-averaged steady fluxes of the solute species to be separated. For the case where the receiving reservoir concentration is small relative to the source reservoir ($C_L \ll C_o$), the selectivity for two solute species A and B is simply the ratio:

$$\frac{N_A}{N_B} = \frac{\exp\left(\frac{L\overline{U}_{BF}}{K_B}\right)-1}{\exp\left(\frac{L\overline{U}_{BF}}{K_A}\right)-1}. \tag{15}$$

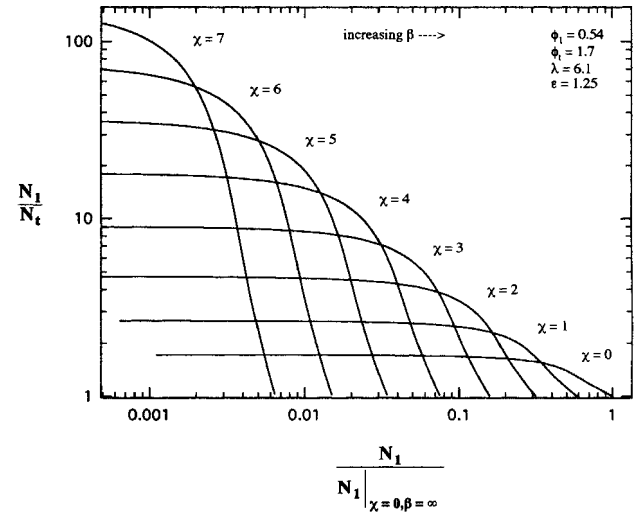

Figure 4. Selectivity as a function of the nondimensionalized throughput of the more strongly absorbing species, where each curve was parameterized by the nondimensional magnitude of the back flow $\chi = \overline{U}_{BF}L/K_1$.

The effect of the back flow is an increased selectivity at the expense of the throughput.

Figure 4 represents the selectivity as a function of the throughput of 1-butanol, where the curves have been parameterized by $\chi = L\overline{U}_{BF}/K$. The parameters ϵ, λ, and ϕ, on which the enhanced diffusivity depends, have the same values as that for our experimental system. It is clear that the selectivity is dramatically improved with back flow, but it does occur at the expense of throughput. By adjusting both the frequency of oscillation and the degree of back flow, it is possible to obtain an optimum transport enhancement for a desired selectivity or selectivity for a desired throughput for fixed values of ϵ, λ, and ϕ.

Experimental

In order to verify the theoretical predictions for the enhancement due to the interactions of wall absorption and fluid oscillations, we chose the model system of the separation of 1-butanol and *t*-butanol from an aqueous solution. The separation was performed using a hollow fiber module (Separations Products Div., Hoechst-Celanese, Charlotte, NC), where the fiber walls were impregnated with *n*-octanol. The hollow fibers were of nominal 234-μm ID, 32.5-μm wall thickness, 20 cm long, and 30% wall porosity. The fiber dimensions were measured using video microscopy and confirmed by pressure/flow rate measurements. The fiber mod-

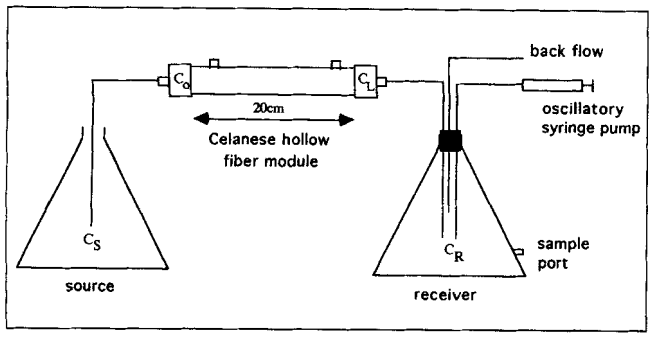

Figure 5. Experimental apparatus.

ule contained 1,730 fibers and was capped at the ends, resulting in dead volume end regions of 15 mL each. The experimental apparatus is presented in Figure 5. The hollow fiber module was in communication with a source and a receiving reservoir. During each experiment the source reservoir initially contained an equimolar aqueous solution of 1-butanol and *t*-butanol, 0.1 M, whereas the receiving reservoir contained distilled water. The volumes of the reservoirs were 1 liter and 1.5 liter for the receiving and source reservoirs, respectively. An oscillatory syringe pump caused the aqueous fluid to oscillate along the length of the fibers. The fluid oscillations were coupled with a steady back flow from the receiving reservoir to the source reservoir to enhance the selectivity of the separation. As the experiment progressed, samples were taken from the receiving and source reservoirs and analyzed with a gas chromatograph.

The Celanese fiber module and the chosen separation fix the parameters ϵ, ϕ, and λ. The partition coefficients of 1-butanol and *t*-butanol were determined by contacting equal volumes of *n*-octanol and an equimolar aqueous solution of 1-butanol and *t*-butanol and measuring the concentration of the aqueous solution after equilibration. Taking into account the porosity of the hollow fiber walls, the following partition coefficients for our model system were found, $\phi_1 = 0.54$ and $\phi_t = 1.7$ (the subscripts of ϕ refer to 1-butanol and *t*-butanol, respectively). The diffusion coefficients for both species in both phases were estimated by the method of Wilke–Chang as well as the Tyne and Calus method (Reid, 1987). Both methods give molecular diffusivities for 1-butanol in *n*-octanol and water that are equal to the molecular diffusivities of *t*-butanol in those phases. On the basis of those estimations, we found that the ratio of the molecular diffusivities in the two phases, λ, was 6.1 for both species. The ratio of the outer to inner radius of the hollow fibers was 1.28. However, while ϵ, ϕ, and λ are fixed by the model system, we could still verify the dependence of the enhancement on the tidal displacement, the frequency, and the magnitude of the back flow.

The analysis of the experimental data to calculate the experimental enhanced axial diffusivity is complicated by the dead volumes in the end caps of the hollow fiber cartridge. These dead volumes give rise to an additional mass transport resistance. The volumes of the tubes connecting the fiber cartridge to the source and receiving reservoirs are smaller than the stroke volumes so that the connecting tubing is not a barrier to mass transfer. The flux can be modeled as the flux between the well-mixed reservoirs and the end caps of the fiber cartridge and the flux across the fiber cartridge. The flux across the hollow fiber cartridge is given by (cf. Eq. 14)

$$\text{flux} = N\,\text{Area} = \bar{U}_{BF}\,\text{Area}\,\frac{C_o - C_L \exp\left(\dfrac{L\bar{U}_{BF}}{K_{\text{exp}}}\right)}{\exp\left(\dfrac{L\bar{U}_{BF}}{K_{\text{exp}}}\right) - 1}. \quad (16)$$

The flux from the source reservoir to the dead volume on the source side of the cartridge is simply that due to fluid motion in the connecting tube. For small back flow and a tidal volume much less than the dead volume, this is given by

$$\text{flux} = (C_S - C_o)\frac{\Delta V \omega}{2\pi} - \frac{\bar{U}_{BF}\,\text{Area}}{2}(C_S + C_o). \quad (17)$$

Similarly, the flux between the receiving reservoir and its corresponding dead volume is given by

$$\text{flux} = (C_L - C_R)\frac{\Delta V \omega}{2\pi} - \frac{\bar{U}_{BF}\,\text{Area}}{2}(C_L + C_R). \quad (18)$$

At steady state all of these fluxes are equal. We thus can use Eqs. 16–18 to eliminate the unknown concentrations C_o and C_L. Let us define

$$z = \frac{\Delta V \omega}{\bar{U}_{BF}\,\text{Area}\,\pi} \quad \text{and} \quad \eta = \exp\left(\frac{L\bar{U}_{BF}}{K_{\text{exp}}}\right) = \exp(\chi).$$

In terms of these variables, the flux is given by

$$\text{flux} = \bar{U}_{BF}\,\text{Area}\,\frac{C_S(z-1)^2(\eta-1) - C_R 2\eta(z+1)^2(\eta-1)}{[\eta+1+z(\eta-1)]^2 - 4\eta}. \quad (19)$$

where C_S and C_R are the measured source and receiving reservoir concentrations, respectively.

The equations just derived are strictly valid only at steady state. In our experiments, however, we are examining the transient response of the source and receiving reservoir concentrations. We shall use the steady-state flux expressions, however, by invoking a pseudo-steady-state approximation. This will be valid because the reservoir volumes are more than 20 times the combined volumes of the fiber cartridge and dead volumes. Thus the time for the fibers to approach steady state is much shorter than the characteristic time scale for changes in the reservoir concentrations.

Due to the small-amplitude back flow and the duration of the experiment, the concentration in the source reservoir changes significantly, and this must be accounted for in the analysis as well. The volume of the source reservoir is given as the sum of the initial volume and that due to the back flow, $V_S = V_o + \bar{U}_{BF}\,\text{Area}\,t$. We can then define the rate of change in the concentration of the source reservoir as

$$\frac{d(V_S C_S)}{dt} = -\text{flux}. \quad (20)$$

Carrying out the derivative on the lefthand side results in the following expression for the rate of change in the source reservoir concentration

$$\frac{dC_S}{dt} = -\frac{\text{flux}}{V_S} - \frac{C_S}{V_S}\bar{U}_{BF}\,\text{Area}. \tag{21}$$

Equivalently, we have for the receiving reservoir concentration,

$$\frac{dC_R}{dt} = \frac{\text{flux}}{V_R}, \tag{22}$$

since V_R is constant. Let us define a nondimensional time $t^* = \bar{U}_{BF}$ Area t/V_o. Substitution of Eq. 19 into Eqs. 21 and 22 gives

$$\frac{dC_S}{dt^*} = -\frac{1}{1+t^*} \times \left\{ \frac{C_S(z+1)^2(\eta-1) - C_R\eta(z+1)^2(\eta-1)}{[\eta+1+z(\eta-1)]^2 - 4\eta} + C_S \right\}. \tag{23}$$

$$\frac{dC_R}{dt^*} = \frac{V_o}{V_R} \frac{C_S(z+1)^2(\eta-1) - C_R\eta(z+1)^2(\eta-1)}{[\eta+1+z(\eta-1)]^2 - 4\eta}. \tag{24}$$

In order to determine the experimental value for the axial diffusivity K_{exp}, a nonlinear regression was performed. The experimentally measured concentration of the receiving reservoir as a function of time was fitted to the solution, C_R, of the coupled ordinary differential equations. Figure 6 is a typical representation of the fit for one of the experiments.

The analysis of the data for experiments without back flow is simplified since the volume of the source reservoir V_S remains constant. In this case the equations for the rate of change of concentration are given as

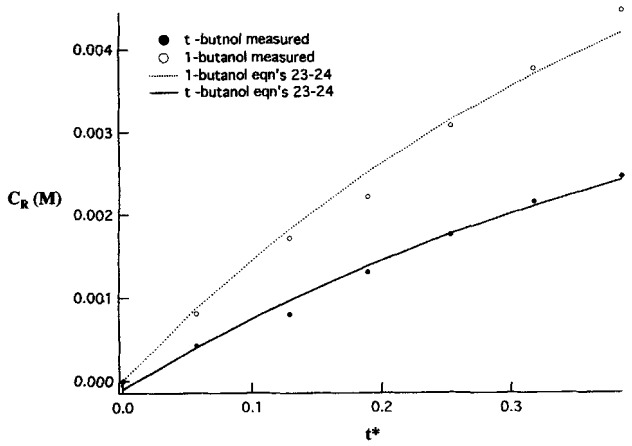

Figure 6. Fit of measured concentrations of 1- and *t*-butanol to the solution of Eqs. 23 and 24.

The stroke volume for this experiment was 9 mL, the back flow 3.69 mL/min, and the frequency of oscillation 0.3 rad/s.

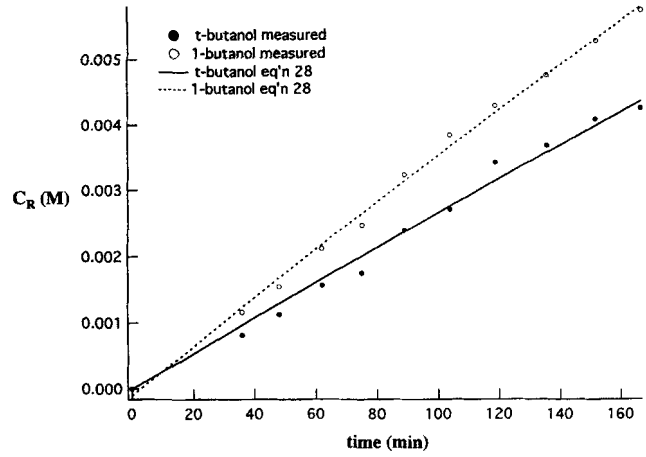

Figure 7. Fit of measured concentrations of 1- and *t*-butanol to the solution of Eq. 27.

The stroke volume for this experiment was 3.9 mL and the frequency of oscillation 0.3 rad/s.

$$\frac{dC_S}{dt} = -\frac{(C_S - C_R)}{V_S} \frac{K_{\text{exp}}\,\text{Area}\;\omega\Delta V}{L\omega\Delta V + 4\pi K_{\text{exp}}\,\text{Area}} \tag{25}$$

$$\frac{dC_R}{dt} = -\frac{(C_S - C_R)}{V_R} \frac{K_{\text{exp}}\,\text{Area}\;\omega\Delta V}{L\omega\Delta V + 4\pi K_{\text{exp}}\,\text{Area}}. \tag{26}$$

With the initial conditions $C_S\,(t=0) = C_{So}$ and $C_R\,(t=0) = C_{Ro}$, we can solve for C_R

$$C_R = -\frac{C_{So} - C_{Ro}}{V_S + V_R} V_S \exp\left(-\frac{K_{\text{exp}}\,\text{Area}\;\omega\Delta V}{L\omega\Delta V + 4\pi K_{\text{exp}}\,\text{Area}} \frac{V_S + V_R}{V_S V_R} \right) + \frac{C_{So}V_S + C_{Ro}V_R}{V_S + V_R}. \tag{27}$$

Again the experimental data are fitted to this curve with a nonlinear regression in order to determine K_{exp}, as shown in Figure 7.

Results

As mentioned before, the tidal displacement, the magnitude of the back flow, and the frequency of oscillation were the only parameters that could be varied in order to verify the enhancement of transport rate predicted by the analytical solution. The magnitude of the stroke volume ranged from 1.62 to 9 mL, which was equivalent to a nondimensional tidal amplitude $\Delta x/L$ ranging from 0.054 to 0.30. The back flow varied from 0.013 to 0.062 mL/s, so that χ_{exp} ranged from 1.06 to 5.11. The oscillation frequencies ranged between 0.3 and 0.7 rad/s.

We know from our analytical solution that the enhancement should be proportional to the square of the tidal displacement Δx. Therefore, the functional dependence of K_{exp} vs. Δx should give a straight line with slope 2 in a log-log graph. As may be seen in Figure 8, the slopes of both curves are 1.86 ± 0.28 and 1.92 ± 0.26 (2σ error) for 1-butanol and *t*-butanol, respectively, which are well within two standard deviations of the theoretical prediction. The magnitude of the

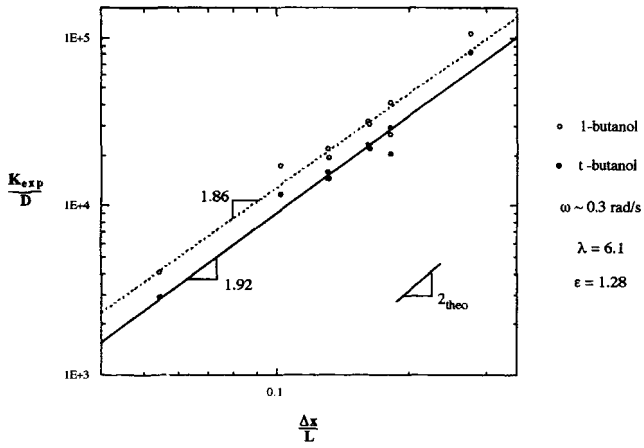

Figure 8. Nondimensionalized experimental enhanced axial diffusivity K as a function of the nondimensional tidal displacement.

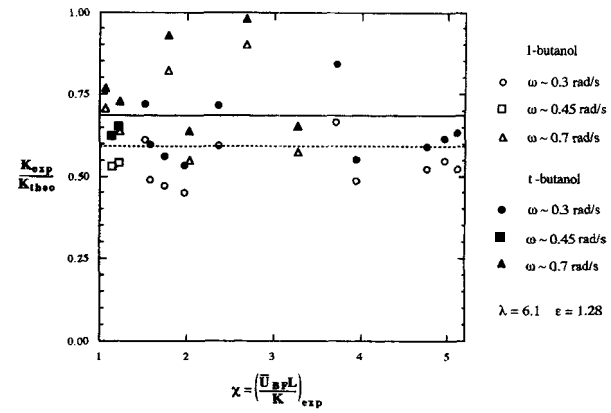

Figure 9. Experimental vs. theoretical predicted enhanced axial diffusivity K as a function of the nondimensional magnitude of the back flow χ for different oscillation frequencies.

The solid and dashed lines are the ratio of the experimental and theoretical enhanced axial diffusivity K averaged over all frequencies for t-butanol and 1-butanol, respectively.

enhancement is on average 1.4 times larger for 1-butanol than t-butanol, indicating that a separation is achieved. Note that we have achieved enhanced axial diffusivities as great as 1.06 $\times 10^5$ times that of molecular diffusion through water.

The theory developed earlier is strictly valid for transport in a cylindrical tube when the tidal displacement, Δx, is much smaller than the length of the tube, L. For slow diffusion in the mobile phase with respect to oscillation frequency, for example, direct convective mixing at the centerline between reservoirs occurs when $\Delta x/L$ exceeds 0.25, and thus we would expect our analysis will begin to break down beyond this point. The largest value for $\Delta x/L$ used in our experiments without back flow was approximately 0.28. Even for such a large value of $\Delta x/L$ the observed transport enhancement and selectivity were close to the theoretically predicted values, suggesting that end effects were relatively unimportant. A similar observation was made by Chandhok and Leighton (1991), who found that end effects were negligible for oscillatory mass transport in a finite-length slug (a somewhat different geometry from that considered here), provided that the bore aspect ratio (a/L) was small.

In Figures 9 and 10 we compare the experimentally observed mass-transfer enhancement to that predicted by our model—which contains no adjustable parameters—for runs with and without back flow, respectively. For the runs without back flow, the enhancement is given as a function of the stroke volume at angular frequencies ranging between 0.3 and 0.7 rad/s. For experiments with back flow, we kept the stroke volume constant and varied the amplitude of the back flow as well as the angular frequency. As may be seen, our experimental enhancement is within a factor of 2 of the predicted value, and the experimental selectivity, while smaller than the theoretical value, is within 14% of the predicted selectivity. From both figures it may be seen that the agreement between the theoretical and experimental enhancement is not significantly affected by the amplitude of the oscillation, the magnitude of the back flow, or the oscillation frequency.

To better understand the effect of back flow on the selectivity and the throughput, it is useful to examine a typical set of experiments. At an angular frequency of 0.3 rad/s, for example, without back flow the theoretically predicted selectivity is 1.6, while that experimentally observed (averaged over all tidal displacements used at that frequency) was 1.4. At the same angular frequency, but with a back flow of 1.8 mL/min and a stroke volume of 3.9 mL ($\chi_{exp} = 3.94$), we observed a 5.6:1 selectivity for 1-butanol (the preferentially absorbed species) and an enhancement in diffusion by a factor of about 22,000-fold. This enhancement was approximately 49% of that predicted theoretically by Eq. 9. The back flow thus increased the selectivity over that observed with no back flow by a factor of ln (5.6)/ln (1.4) = 5.1. At the same time the back flow decreased the throughput by a factor of 0.078. The overall throughput of 1-butanol is thus equivalent to that diffusing through a stagnant film of water of the same area approximately 118 μm thick.

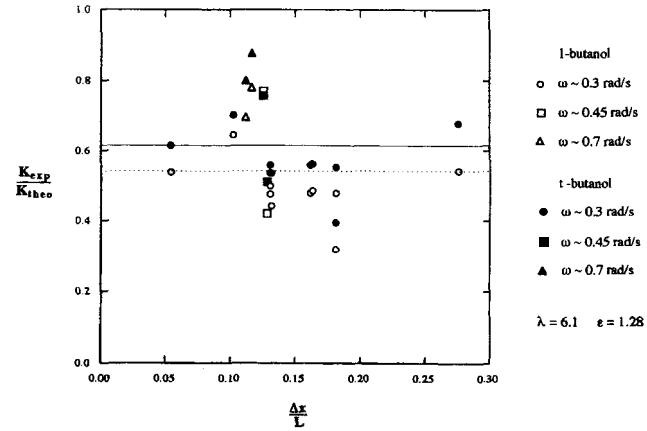

Figure 10. Experimental vs. theoretical predicted enhanced axial diffusivity K as a function of the nondimensional tidal amplitude for different oscillation frequencies and no back flow.

The solid and dashed lines are the ratio of the experimental and theoretical enhanced axial diffusivity K averaged over all frequencies for t-butanol and 1-butanol, respectively.

It is unclear what the source of the discrepancy between the measured and predicted enhancements may be attributed to. Possible sources of error include errors in the porosity of the hollow fibers, the assumed tortuosity of 1 (used in the estimation of D_s), and the measured stroke volume. The porosity for the fibers was assumed to be 30%—an estimate provided by the manufacturer—as we could not reliably measure this quantity. A smaller porosity (larger ϕ) and/or tortuosity greater than one would result in a smaller enhancement than predicted by the assumed values. As may be seen from Figure 3, the effect on the magnitude of the enhancement is larger than the effect on the selectivity which, if this were the source of discrepancy, is qualitatively consistent with our experimental observations. This is similarly true of errors in the stroke volume measurements. A 20% overestimation in the amplitude of the stroke volume alone would be sufficient to account for the discrepancy, given the dependence of the enhancement on the square of the tidal displacement. Additionally, errors in the fiber radius and number of fibers also would greatly affect the theoretical predictions.

Discussion

The hollow fiber module employed in the experiment described in the previous sections is only a model system and is not necessarily practical for large-scale separations. What are of particular interest, however, are the scaling laws that govern the throughput and membrane size for the coupling of fluid oscillations with wall absorption. From the transport equations we can show that the device can be scaled down in fiber length and size without affecting the mass transport. The solute flux across an individual fiber bore is given by

$$N = -K\frac{\partial C}{\partial x}, \tag{28}$$

where K scales as $D(\Delta x/L)^2(L/a)^2 f(\beta,\epsilon,\lambda,\phi)$. Therefore, the throughput of the solute per unit area of membrane, Q/A, for a linear concentration profile is

$$\frac{Q}{A} = D\left(\frac{\Delta x}{L}\right)^2 Lf(\beta,\epsilon,\lambda,\phi)\Delta C\frac{\theta}{a^2}, \tag{29}$$

where θ denotes the fraction of the membrane surface occupied by the fiber bore. Note that for a fixed nondimensional amplitude of oscillation ($\Delta x/L$) this flux can be increased by either decreasing a or increasing L. Unfortunately, the maximum allowable pressure drop across the fibers imposes limits on the bore radius and the fiber length. This pressure drop is given as $\Delta P = [(8\Delta x\omega)/a^2]L\mu$, where μ is the viscosity of the oscillating fluid. Therefore, from the definition $\omega = \beta^2(D/a^2)$, the square of the minimum pore radius scales as

$$\beta L\left(\frac{\Delta x}{L}\frac{8D\mu}{\Delta P}\right)^{1/2}.$$

The resulting expression for the throughput is simply

$$\frac{Q}{A} = \left(\frac{\Delta x}{L}\right)^{3/2}\left(\frac{D\Delta P}{8\mu}\right)^{1/2}\frac{f(\beta,\epsilon,\lambda,\phi)}{\beta}\Delta C\theta, \tag{30}$$

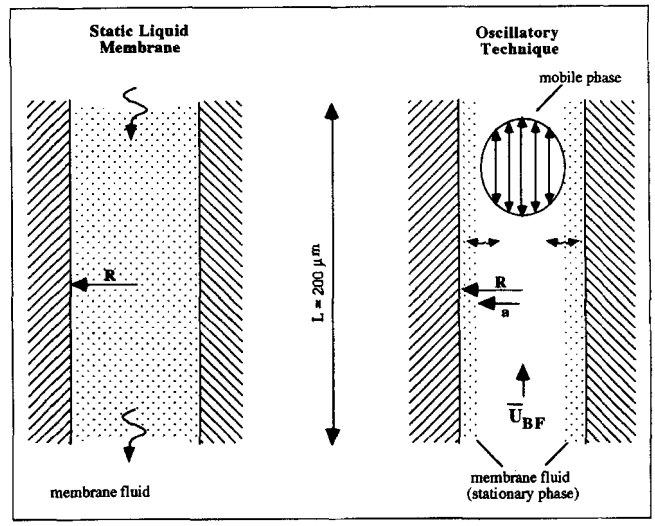

Figure 11. Pore of a solid support using the support for a conventional static liquid membrane or oscillatory chromatography.

In the case of oscillatory chromatography only the walls are coated with the same membrane fluid that fills the pore completely for the conventional static liquid membrane. In contrast to the static membrane, the throughput and selectivity can be varied for oscillatory chromatography.

showing clearly that for a constant maximum pressure drop and oscillation frequency β the performance of the separation device is independent of the total length and inner radius of the fibers. We may thus decrease the total bore volume per unit area θL without changing the throughput. This scaling down is useful in reducing the required amount of solvent for the stationary phase.

On the basis of these scaling arguments, we have compared the theoretical performance of oscillatory chromatography to that of an ordinary liquid membrane, each with the same support structure. Figure 11 shows the "pore" configuration for both cases. In the case of the conventional membrane, the pores are completely filled and the flux is limited by the diffusion rate. As mentioned earlier, the selectivity is determined by the relative affinity of the solute for the membrane fluid. For oscillatory chromatography, however, the walls of the pores are coated with a thin stationary phase and the transport rate is governed by the fluid oscillations and the selective reversible absorption in the stationary phase. For comparison a constant pressure drop of atmosphere and a constant $\Delta x/L$ of 0.25 were picked. We selected a support 200 μm thick, a reasonable value for the thickness of a conventional supported liquid membrane. The separation we chose for the comparison was the same as for our experiments.

In order to compare the performance of both techniques, the ratio of the throughput of oscillatory chromatography and the conventional membrane approach is presented in Figure 12 as a function of the ratio of the selectivity of the oscillatory chromatography and the conventional membrane. Assuming that the concentration of both species in the source reservoir is unity and that the concentration in the receiving reservoir is much smaller than one, the selectivity for the conventional membrane is given as $(N_1/N_t)_{con} = \phi_t/\phi_1$. The

throughput of 1-butanol for the conventional membrane is given as $Q_{con} = D_s \pi R^2/(L\phi_1)$, where D is the molecular diffusivity of the solute in the octanol. Similarly, the selectivity for oscillatory chromatography is given as

$$\left(\frac{N_1}{N_t}\right)_{osc} = \frac{\exp\left(\frac{\bar{U}_{BF}L}{K_t}\right)-1}{\exp\left(\frac{\bar{U}_{BF}L}{K_1}\right)-1}, \tag{31}$$

where K_1 and K_t are the enhanced axial diffusion coefficients for 1-butanol and t-butanol. The throughput for 1-butanol for oscillatory chromatography is

$$Q_{osc} = \frac{\bar{U}_{BF}\pi a^2}{\exp\left(\frac{\bar{U}_{BF}L}{K_1}\right)-1}. \tag{32}$$

In Figure 12 the relative selectivity is plotted vs. the relative throughput as a function of the oscillation frequency, for fixed values of $\chi = L\bar{U}_{BF}/K$ ranging from $\chi = 1$ to 8. In order to keep the maximum pressure drop across the pore constant at 1 atmosphere for fixed nondimensional tidal amplitude and pore length, the radius, a, of the mobile phase of the oscillatory technique was varied as a function of ω. For this particular comparison we chose $\epsilon = 1.05$ as the relative thickness of the coating, which means that the volume of the coating on the wall for oscillatory chromatography is only 10% of the volume of membrane fluid in the conventional membrane pore. It may be seen that when both methods have the same selectivity, the oscillatory chromatography has a throughput that is two orders of magnitude better than the throughput of the ordinary membrane. Also, when both methods have the same throughput, the selectivity of the oscillatory chromatography is two orders of magnitude better than the selectivity of the ordinary membrane. In conclusion, there is an envelope, defined by the dashed line along the edge of the curves and the dashed lines at which the techniques have the same selectivity and the same throughput, that describes a wide range of operating conditions for oscillatory chromatography such that it will perform better than the conventional liquid membrane. The dashed line along the edge of the curves defines the optimum operating conditions for the indicated set of fixed parameters. The area to the right of this line, for these parameters, is not accessible. Note, however, the performance of the proposed technique can easily be improved by allowing a larger pressure drop across the membrane and thus smaller radii and higher oscillation frequencies.

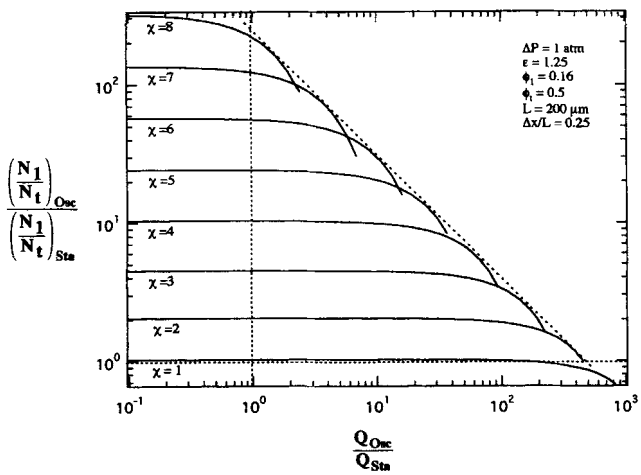

Figure 12. Performance of oscillatory chromatography and a static liquid membrane; the ratio of the selectivity of the two methods as a function of the ratio of throughputs of the two techniques, where each curve was parameterized by the nondimensional magnitude of the back flow χ.

The dashed line along the edges of the curves represents the optimum operating conditions for oscillatory chromatography.

It should be pointed out that the proposed technique has significant limitations. This technique is mainly useful if the relative affinity difference of the species to be separated is not too large and/or if a conventional liquid membrane needs to be relatively thick in order to be stable. A large relative affinity difference and/or a thinner membrane will reduce the envelope of operating conditions where oscillatory chromatography may perform better than an ordinary static liquid membrane. However, we believe there exists a window of separations where this technique is applicable and beneficial. The proposed technique allows the use of less chemically selective, thicker (more stable) membrane systems to achieve the same throughput/selectivity as a more difficult chemical separation.

Conclusions

In this article, we have described a new technique for the separation of solutes with similar molecular diffusivities by coupling fluid oscillations with a reversible selective absorption in the stationary phase. We have presented a model—which contains no adjustable parameters—that predicts the enhancement in transport. The predictions have been qualitatively confirmed by experiments in which 1-butanol and t-butanol were separated from an aqueous solution by imposing fluid oscillations across a hollow fiber module where the fibers were impregnated with n-octanol. We achieved enhancements in transport as high as 10^5. Employing a low-amplitude back flow results in an increase of selectivity at the expense of throughput, as is clearly shown by Figure 4.

Note that the Celanese fiber cartridge, while convenient to use for experimentally verifying the theoretical prediction, is not a practical separation device for our proposed technique. Naturally, the performance of the cartridge used as an oscillatory chromatograph cannot be compared to the flux and selectivity across the fiber wall. It is also not very useful to compare it to a conventional membrane. Instead, as may be gleaned from the scaling discussion, a more practical device can be designed such that it will perform better than a conventional membrane.

It is important to note that we have assumed diffusion-limited processes. This is a valid assumption for our experi-

mental system. Our work could be extended to include a nonlinear reaction term as well as competition effects for lean carrier systems. In these cases, however, no analytical solutions are possible and numerical analysis is required.

In conclusion, the technique described here shows great promise for diffusional separation processes. It is mainly beneficial for separations where the relative difference in affinity for the stationary phase is not too large or where a membrane must be relatively thick in order to be stable. Oscillatory chromatography offers a trade-off in the complexity of chemistry or operating conditions. The experimental separation of 1-butanol and *t*-butanol suggests that the method may be applicable for the separation of enantiomers. Like 1-butanol and *t*-butanol, enantiomers have the same molecular diffusivities, but they have different affinities for chiral acceptor molecules that can be incorporated in the stationary phase of the oscillatory chromatograph. Application to actual enantiomeric systems is the current focus of our research and will be reported in future work.

Notation

A = superficial area over which flux occurs (Eqs. 29, 30)
C = solute concentration in the mobile phase
r = radial coordinate (Figure 1)
t = time
V_i = volume of reservoir i (source, receiving) (Eqs. 20–22, 25–27)
β = nondimensional frequency for a cylinder $a(\omega/D)^{1/2}$
χ = measure of the magnitude of the amplitude of the back flow
ΔP = pressure drop along the length of the fibers
ΔV = oscillatory stroke volume (Eqs. 17, 18, 25–27)

Literature Cited

Aris, R., "On the Dispersion of a Solute in Pulsating Flow through a Tube," *Proc. R. Soc. London A*, **259**, 370 (1960).

Chandhok, A. K., "Oscillatory Separation Processes," PhD Diss. Dept. of Chemical Engineering, Univ. of Notre Dame, Notre Dame, IN (1992).

Chandhok, A. K., N. Voorhies, M. J. McCready, and D. T. Leighton, Jr., "Measurement of Transport Enhancement in Oscillatory Liquid Membranes," *AIChE J.*, **36**(8), 1259 (1990).

Chandhok, A. K., and D. T. Leighton, Jr., "The Influence of End Effects on Mass Transfer in Oscillatory Flows," *Chem. Eng. Sci.*, **46**(10), 2661 (1991).

Ding, H., M.-C. Yang, D. Schisla and E. L. Cussler, "Hollow-Fiber Liquid Chromatography," *AIChE J.*, **35**(5), 814 (1989).

Hertz, G., "About Separations of Gas Mixtures by Diffusion in a Flowing Gas," *Z. Phys.*, **19**, 35 (1923).

Jaeger, M. J., P. Kalle, and U. H. Kurzweg, "Separation of Gases by Enhanced Upstream Diffusion," *Sep. Sci. Technol.*, **27**(6), 691 (1992).

Kurzweg, U., "Enhanced Heat Conduction in Oscillating Viscous Flows within Parallel-Plate Channels," *J. Fluid Mech.*, **156**, 291 (1985).

Leighton, D. T., Jr., and M. J. McCready, "Shear Enhanced Transport in Oscillatory Liquid Membrane," *AIChE J.*, **34**(10), 1709 (1988).

Reid, R. C., J. M. Prausnitz, and B. E. Poling, *The Properties of Gases and Liquids*, 4th ed., McGraw-Hill, New York (1987).

Watson, E. J., "Diffusion in Oscillatory Pipe Flow," *J. Fluid Mech.*, **133**, 233 (1983).

Appendix: Enhanced Axial Diffusion Coefficient, *K*

The solution for the enhanced axial diffusion coefficient in the liquid was obtained by applying the method of moments to the basic transport Eqs. 1–3 with their appropriate boundary conditions (Eqs. 4 and 5). The moments of C are defined as follows for the liquid phase

$$C_p = \int_{-\infty}^{\infty} C(r,x,t)x^p\,dx \tag{A1}$$

for the stationary phase

$$C_p^S = \int_{-\infty}^{\infty} C_S(r,x,t)x^p\,dx \tag{A2}$$

and the combined moment

$$m_p = 2\int_0^a C_p r\,dr + 2\int_a^R C_p^S r\,dr. \tag{A3}$$

It is assumed that the cylinders are infinitely long and that initially ($t = 0$) the solute is confined to a finite length of the tube and distributed uniformly across the plane in each phase and that the two phases are at equilibrium. If we choose C_0^S to be unity, then at $t = 0$ we have the following initial conditions

$$C_0 = \phi, \quad C_0^S = 1, \quad \text{and} \quad m_0 = \phi a^2 + (R^2 - a^2) \tag{A4}$$

and

$$C_p = 0, \quad C_p^S = 0, \quad \text{and} \quad m_p = 0 \quad \text{for} \quad p > 0 \text{ when } t = 0. \tag{A5}$$

We chose the following nondimensionalization

$$t^* = \omega t \qquad r^* = \frac{r}{a} \quad \text{where} \quad \frac{R}{a} = \epsilon.$$

Multiplying Eqs. 1–5 with x^p and integrating with respect to x from $-\infty$ to $+\infty$, we have

$$\frac{\partial C_p}{\partial t^*} - p\frac{2\overline{U}}{\omega}(1 - r^{*2})\cos t^* C_{p-1} = \frac{D}{a^2\omega r^*}\frac{\partial}{\partial r^*}\left(r^*\frac{\partial C_p}{\partial r^*}\right) \tag{A6}$$

$$\frac{\partial C_p^S}{\partial t^*} = \frac{D_S}{a^2\omega r^*}\frac{\partial}{\partial r^*}\left(r^*\frac{\partial C_p^S}{\partial r^*}\right) \tag{A7}$$

B.C.'s

$$\phi C_p^S|_{r^*=1} = C_p|_{r^*=1} \tag{A8}$$

$$D_S\left.\frac{\partial C_p^S}{\partial r^*}\right|_{r^*=1} = D\left.\frac{\partial C_p}{\partial r^*}\right|_{r^*=1} \tag{A9}$$

$$\left.\frac{\partial C_p}{\partial r^*}\right|_{r^*=0} = 0 = \left.\frac{\partial C_p^S}{\partial r^*}\right|_{r^*=\epsilon}. \tag{A10}$$

Multiplying Eqs. A6–A7 by $2r$ and integrating Eq. A6 with respect to r from 0 to a and Eq. A7 from a to R, we find

$$a^2\frac{\partial}{\partial t^*}\int_0^1 2C_p r^* dr^* - a^2 p\frac{2\overline{U}}{\omega}\cos t^*\int_0^1 2(1-r^{*2})C_{p-1}r^*\,dr^* = 2\frac{D}{\omega}\frac{\partial C_p}{\partial r^*}\bigg|_{r^*=1} \quad \text{(A11)}$$

$$a^2\frac{\partial}{\partial t^*}\int_1^\epsilon 2C_p^S r^*\,dr^* = -2\frac{D_S}{\omega}\frac{\partial C_p^S}{\partial r^*}. \quad \text{(A12)}$$

Adding Eqs. A11 and A12 and using condition 14, we get

$$\frac{\partial m_p}{\partial t^*} = a^2 p\frac{2\overline{U}}{\omega}\cos t^*\int_0^1 2(1-r^{*2})C_{p-1}r^*\,dr^*. \quad \text{(A13)}$$

Because we are dealing with oscillatory flow, the distribution tends to normality and the first two moments are sufficient to describe the distribution. In order to solve for m_2, we only need to solve Eqs. A6–A10 for $p = 0, 1$. It is clear that for $p = 0$, Eq. A13 gives

$$\frac{\partial m_o}{\partial t^*} = 0,$$

which simply states that m_o is constant, $m_o = a^2[\phi + (R^2 - a^2)/a^2]$. This is just a statement of the conservation of solute. The initial conditions ($p = 0$) also satisfy Eqs. A6–A10. We can now solve Eq. A13 for $p = 1$. Inserting the initial condition A4 and condition A5 gives

$$\frac{\partial m_1}{\partial t^*} = a^2\frac{2\overline{U}}{\omega}\cos t^*\int_0^1 2(1-r^{*2})\phi r^*\,dr^*$$

$$\therefore m_1 = \frac{\phi a^2 2\overline{U}}{2\omega}\sin t^*. \quad \text{(A14)}$$

All that is needed now is to solve Eq. A13 for $p = 2$,

$$\frac{\partial m_2}{\partial t^*} = 2a^2\frac{2\overline{U}}{\omega}\cos t^*\int_0^1 2(1-r^{*2})C_1 r^* dr^*, \quad \text{(A15)}$$

but first we have to solve Eqs. A6–A10 for $p = 1$ to find the solution for C_1.

Setting $p = 1$ and inserting the initial values for C (Eqs. A4–A5) into Eqs. A6 and A7 we obtain the following set of equations:

$$\frac{\partial C_1}{\partial t^*} - \phi\frac{2\overline{U}}{\omega}(1-r^{*2})\cos t^* = \frac{D}{a^2\omega r^*}\frac{\partial}{\partial r^*}\left(r^*\frac{\partial C_1}{\partial r^*}\right) \quad \text{(A16)}$$

$$\frac{\partial C_1^S}{\partial t^*} = \frac{D_S}{a^2\omega r^*}\frac{\partial}{\partial r^*}\left(r^*\frac{\partial C_1^S}{\partial r^*}\right). \quad \text{(A17)}$$

B.C.'s

$$\phi C_1^S|_{r^*=1} = C_1|_{r^*=1} \quad \text{(A18)}$$

$$D_S\frac{\partial C_1^S}{\partial r^*}\bigg|_{r^*=1} = D\frac{\partial C_1}{\partial r^*}\bigg|_{r^*=1} \quad \text{(A19)}$$

$$\frac{\partial C_1}{\partial r^*}\bigg|_{r^*=0} = 0 = \frac{\partial C_1^S}{\partial r^*}\bigg|_{r^*=\epsilon}. \quad \text{(A20)}$$

Let us define the following nondimensional parameters

$$\lambda = \frac{D}{D_S} \qquad \frac{a^2\omega}{D} = \beta^2 \qquad \frac{a^2\omega}{D_S} = \lambda\beta^2.$$

We can also write $\cos t^*$ in terms of complex variables, $\cos t^* = Re\{e^{it^*}\}$, where $i = \sqrt{-1}$, keeping in mind that only the real part of the resulting solution has physical significance. Accordingly, we then define C in terms of complex variables, $C_1^n = Re\{f_n(r^*)e^{it^*}\}$, where n indicates the phase under consideration. Finally, we can expand the righthand term in Eqs. A16 and A17 as

$$\frac{1}{r^*}\frac{\partial}{\partial r^*}\left(r^*\frac{\partial C_1^n}{\partial r^*}\right) = \frac{1}{r^{*2}}\left(r^*\frac{\partial C_1^n}{\partial r^*} + r^{*2}\frac{\partial^2 C_1^n}{\partial r^{*2}}\right).$$

Using the preceding, we can rewrite Eqs. A16 and A17 as

$$r^{*2}f'' + r^* f' - ir^{*2}f\beta^2 = -\frac{\beta^2\phi 2\overline{U}}{\omega}(1-r^{*2})r^{*2} \quad \text{(A21)}$$

$$r^{*2}f_S'' + r^* f_S' - ir^{*2}f_S\lambda\beta^2 = 0, \quad \text{(A22)}$$

where the single and double prime refer to the first and second derivative with respect to r, respectively. The solution for f contains a particular and a homogeneous part, $f = f_H + f_p$. The following particular solution satisfies Eq. A21

$$f_p = \frac{\phi 2\overline{U}}{\omega}\left[\frac{4}{\beta^2} + i(r^{*2}-1)\right]. \quad \text{(A23)}$$

The homogeneous equations, Eqs. A21 and A22 have the form of Bessel equations and the solutions are given in terms of Bessel functions

$$f_H = A_1 J_0(i^{3/2}\beta r^*) + B_1 K_0(i^{1/2}\beta r^*) \quad \text{(A24)}$$

$$f_s = A_2 J_0(i^{3/2}\sqrt{\lambda}\,\beta r^*) + B_2 K_0(i^{1/2}\sqrt{\lambda}\,\beta r^*) \quad \text{(A25)}$$

where A_i and B_i are constants to be determined. Given the expressions for f_n we can determine the form of f_n'

$$f' = A_1[\mathrm{ber}_1(\beta r^*) + \mathrm{bei}_1(\beta r^*) - i\,\mathrm{ber}_1(\beta r^*) + i\,\mathrm{bei}_1(\beta r^*)]\frac{\beta}{\sqrt{2}}$$
$$+ B_1[\mathrm{ker}_1(\beta r^*) + \mathrm{kei}_1(\beta r^*) - i\,\mathrm{ker}_1(\beta r^*)$$
$$+ i\,\mathrm{kei}_1(\beta r^*)]\frac{\beta}{\sqrt{2}} + 2i\frac{\phi 2\overline{U}}{\omega}r^* \quad \text{(A26)}$$

$$f'_s = A_2[\mathrm{ber}_1(\sqrt{\lambda}\,\beta r^*) + \mathrm{bei}_1(\sqrt{\lambda}\,\beta r^*) - i\,\mathrm{ber}_1(\sqrt{\lambda}\,\beta r^*) + i\,\mathrm{bei}_1(\sqrt{\lambda}\,\beta r^*)]\frac{\sqrt{\lambda}\,\beta}{\sqrt{2}} + B_2[\mathrm{ker}_1(\sqrt{\lambda}\,\beta r^*) + \mathrm{kei}_1(\sqrt{\lambda}\,\beta r^*) - i\,\mathrm{ker}_1(\sqrt{\lambda}\,\beta r^*) + i\,\mathrm{kei}_1(\sqrt{\lambda}\,\beta r^*)]\frac{\sqrt{\lambda}\,\beta}{\sqrt{2}}. \quad \text{(A27)}$$

The boundary conditions (Eqs. A18–A20) provide us with four equations to solve for the four unknowns

$$f'(0) = 0 \quad \therefore B_1 = 0 \quad \text{(A28)}$$

$$f'_s(\epsilon) = 0 \quad \therefore A_2 = iB_2\frac{K_1(i^{1/2}\sqrt{\lambda}\,\epsilon\beta)}{J_1(i^{3/2}\sqrt{\lambda}\,\epsilon\beta)} \quad \text{(A29)}$$

$$\phi f_s(1) = f(1) \;\therefore A_1 J_0(i^{3/2}\beta) + \frac{4\phi 2\overline{U}}{\omega\beta^2} = \phi[A_2 J_0(i^{3/2}\sqrt{\lambda}\,\beta) + B_2 K_0(i^{1/2}\sqrt{\lambda}\,\beta)] \quad \text{(A30)}$$

$$f'_s(1) = \lambda f'(1) \;\therefore \sqrt{\lambda}A_1 J_1(i^{3/2}\beta)(1-i) + i\frac{2\sqrt{2}\,\phi\sqrt{\lambda}\,2\overline{U}}{\omega\beta} = A_2 J_1(i^{3/2}\sqrt{\lambda}\,\beta)(1-i) - iB_2 K_1(i^{1/2}\sqrt{\lambda}\,\beta)(1-i). \quad \text{(A31)}$$

From the preceding, we get the expression for A_1

$$A_1 = -\frac{\phi 2\overline{U}}{\omega\beta^2}\frac{\phi\sqrt{\lambda}\,\beta\sqrt{2}\,(1+i)G + 4H}{J_0(i^{3/2}\beta)H - i\sqrt{\lambda}\,\phi J_1(i^{3/2}\beta)G}, \quad \text{(A32)}$$

where

$$H = J_1(i^{3/2}\sqrt{\lambda}\,\epsilon\beta)K_1(i^{1/2}\sqrt{\lambda}\,\beta) - J_1(i^{3/2}\sqrt{\lambda}\,\beta)K_1(i^{1/2}\sqrt{\lambda}\,\epsilon\beta)$$

$$G = J_1(i^{3/2}\sqrt{\lambda}\,\epsilon\beta)K_0(i^{1/2}\sqrt{\lambda}\,\beta) + iJ_0(i^{3/2}\sqrt{\lambda}\,\beta)K_1(i^{1/2}\sqrt{\lambda}\,\epsilon\beta).$$

Finally, we can write the expression for C_1 as

$$C_1 = Re\left\{\left(A_1 J_0(i^{3/2}\beta r^*) + \frac{\phi 2\overline{U}}{\omega}\left[\frac{4}{\beta^2} + i(r^{*2}-1)\right]\right)e^{it^*}\right\}.$$

Now that we have solved for C_1 we can go back to Eq. A15 and solve for the second moment. Note that only the real part of $e^{it^*} = \cos t^* + i \sin t^*$ will contribute to the time-averaged variance since $\langle \cos t^* \sin t^* \rangle = 0$, whereas $\langle \cos t^* \cos t^* \rangle = 0.5$. Thus, we can write

$$\frac{\partial\dfrac{m_2}{m_o}}{\partial t} = \frac{2\omega\left(\dfrac{2\overline{U}}{\omega}\right)}{\left[\phi + \dfrac{R^2-a^2}{a^2}\right]}\int_0^1 (1-r^{*2})r^* Re\left\{A_1 J_0(i^{3/2}\beta r^*) + \frac{\phi 2\overline{U}}{\omega}\left[\frac{4}{\beta^2} + i(r^{*2}-1)\right]\right\}dr^*, \quad \text{(A33)}$$

where

$$\int_0^1 (1-r^{*2})r^* Re\left\{\frac{\phi 2\overline{U}}{\omega}\left[\frac{4}{\beta^2} + i(r^{*2}-1)\right]\right\}dr^* = \frac{\phi 2\overline{U}}{\omega\beta^2}$$

$$\int_0^1 (1-r^{*2})r^* J_0(i^{3/2}\beta r^*)dr^* = \frac{4}{\sqrt{2}\,\beta^3}J_1(i^{3/2}\beta)(1-i) - \frac{2i}{\beta^2}J_0(i^{3/2}\beta).$$

Let

$$F = \frac{4}{\sqrt{2}\,\beta^3}J_1(i^{3/2}\beta)(1-i) - \frac{2i}{\beta^2}J_0(i^{3/2}\beta)$$

$$B = \frac{\phi\sqrt{\lambda}\,\beta\sqrt{2}\,(1+i)G + 4H}{J_0(i^{3/2}\beta)H - i\sqrt{\lambda}\,\phi J_1(i^{3/2}\beta)G},$$

then

$$\frac{\partial\dfrac{m_2}{m_o}}{\partial t} = \frac{2\omega\left(\dfrac{2\overline{U}}{\omega}\right)^2}{\left[\phi + \dfrac{R^2-a^2}{a^2}\right]}\frac{\phi}{\beta^2}[1 - Re\{BF\}]. \quad \text{(A34)}$$

Note that the preceding is the variance for both phases; multiplying Eq. A34 by

$$\frac{1}{2}\left[1 + \frac{R^2-a^2}{\phi a^2}\right]$$

gives the enhanced axial diffusion coefficient for the mobile phase

$$K = 4\frac{\Delta x^2\omega}{\beta^2}\left(1 - Re\left\{A\left[\frac{4}{\sqrt{2}\,\beta^3}J_1(i^{3/2}\beta)(1-i) - \frac{2i}{\beta^2}J_0(i^{3/2}\beta)\right]\right\}\right), \quad \text{(A35)}$$

where $\Delta x = \overline{U}/\omega$. The flux of solute species between two reservoirs at concentrations differing by ΔC, connected by hollow fibers length L whose walls have been impregnated with a solvent that selectively absorbs a solute, is thus given as

$$N = K\Delta C/L. \quad \text{(A36)}$$

Manuscript received Jan. 25, 1994, and revision received May 30, 1995.